6. SIMPLIFIED UHPC JOINTS FOR BRIDGE CONSTRUCTION

6.1. OVERVIEW

This chapter investigates the use of UHPC for bridge joint connections between precast, regular concrete bridge deck elements. The proposed joints make use of UHPC's superior bond characteristics in order to provide a simple and effective method for the assembly of precast bridge elements. A total of 12 beams with joint widths of 4" (100 mm), 6" (150 mm), and 8" (200 mm) were constructed for physical testing and subsequently modeled. Of the twelve, 8 beams were tested under pure flexure. The four remaining beams were evaluated under combined shear and flexure loading conditions. Findings show that the beams with joint widths of 4" (100 mm) failed to sufficiently transfer load between the precast desks in both pure flexure and combined shear and flexure testing, resulting in splitting failure in the joint. Beams with joints at 6" (150 mm) and 8" (200 mm) were sufficient for achieving the required force transfer between the precast deck elements and were suitable for applications requiring simplified and expedited construction. Finite element simulations used to explore the effect of joint topology on system performance indicate that structural response hardly changes for the three types of joints considered.

6.2. DESIGN OF THE EXPERIMENTAL PROGRAM

As seen in Chapter 5, UHPCs exceptional ability to bond to steel bar reinforcement allows for small bar development lengths and, therefore, splice lengths. This characteristic enables smaller and simpler joints, which promote accelerated bridge construction methods. The objective of the

test program in this chapter is to probe the lower limits of joint size in order to gain a better understanding of UHPC joint response.

6.2.1. Pure Flexure vs. Combined Shear and Flexure Testing

Two different testing set ups were implemented in this study. The first, a four-point bending test set up seen in Figure 6-1a places the UHPC joint in pure flexure. The second test type, an offset three-point bending set up (Figure 6-1b), subjects the UHPC joint to shear forces and moments. The shear and moments that develop along the length of the beam during testing are shown in Figure 6-1. The pure flexure test is intended to study the response of the joined beam under real world loading conditions where the influence of shear force is minimal. The combined shear and flexure test investigates response when a higher shear-moment ratio is present.

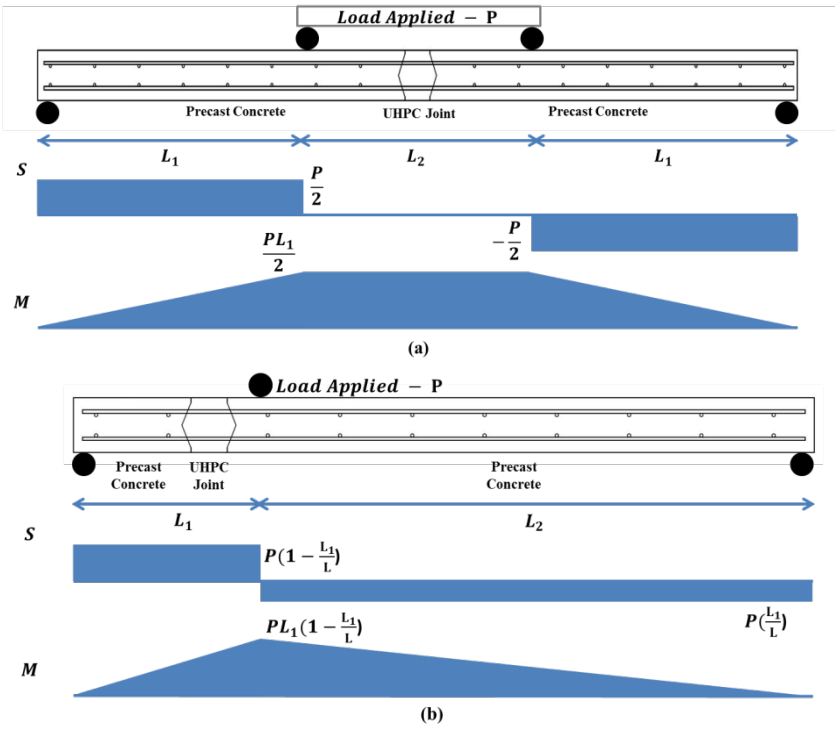

Figure 6-1: Shear and Moment forces in beams under (a) pure flexure loading and (b) combined shear and flexure testing

6.2.2. Joint Details & Selection

Currently the width of a joint for lap splice connection is determined by the lap length which is a function of the development length of the reinforcing bar, and is prescribed by ACI Committee 318 (2005). Equation 6-1 shows the current method for determining the development length for straight bar reinforcement for #6 (19 mm) bars and smaller:

$$L_d = \frac{f_y \psi_t \psi_e \lambda}{25\sqrt{f_c'}} d_b$$

Equation 6-1: Development Length for Straight Bar Reinforcement (ACI 318)

Where f_y = yield strength of the reinforcement (psi), ψ_t = reinforcement location factor, ψ_e = reinforcement coating factor, λ = lightweight concrete aggregate factor, f_c' = compressive strength of the concrete, and d_b = nominal diameter of the bar reinforcement. Equation 6-1 indicates that the required development length decreases with the square root of the compressive strength of the material. Although not explicitly developed or permitted for use with UHPC, it is interesting to note that the bond required for 25 ksi UHPC versus a regular 5 ksi concrete should be just under half of that required for regular concrete according to Equation 6-1.

Similarly, AASHTO LFRD design requires a development length for No. 11 bars or smaller to equal:

$$l_{db} = \frac{1.25 A_b f_y}{\sqrt{f_c'}}$$

Where A_b is the area of the bar in in2, f_y is the specified yield strength of the reinforcing bars (ksi) , f'_c is the specified compressive strength of the concrete at 28 days (ksi) and d_b is diameter of the bar in inches.

6.2.3. Specimen Design

For ease of construction, non-contact lap splices are used in this study. Generally, contact lap splices are constructed such that the reinforcing bars are touching and tied together, minimizing displacements during the pouring of concrete. This is not a concern in precast element constructions as the bars are already embedded in the precast concrete and not able to move in relation to each other. While the new low-cost alternative UHPC mix formulations used in this study have lower material costs than previous UHPC mixes, it is important to minimize the joint width as the alternative UHPC used to fill the joint still carries a higher cost as compared to conventional concrete.

Figure 6-2 shows the reinforcement and joint details for the specimens studied. For the pure flexure tests, each precast deck element measures 60” (1500 mm) in length, 18” (457 mm) wide and 6” (150 mm) deep. Joint lengths vary between 4”, 6” and 8” (100, 150 and 200 mm). Longitudinal reinforcement is spaced at 6.3” (160 mm) along the width of the deck. Transverse reinforcement is spaced at 7.8” (200 mm) along the length of the deck. Reinforcement at the lower layer is placed at a depth of 3.5” (89 mm) and 1.5” (39 mm) for the upper layer.

Similarly, for the combined shear and flexure specimens, one of the precast deck element measures 60” (1500 mm) in length, 18” (457 mm) wide and 6” (150 mm) deep. The other precast

element measures 13” (330 mm) long, with a width of 18” (457 mm) and depth of 6” (150 mm). Joint width is held constant at 4” (100 mm). Longitudinal reinforcement is spaced at 6.3” (160 mm) along the width of the deck. Transverse reinforcement is spaced at 7.8” (200 mm) along the length of the deck. Reinforcement at the lower layer is placed at a depth of 3.5” (89 mm) and 1.5” (39 mm) for the upper layer.

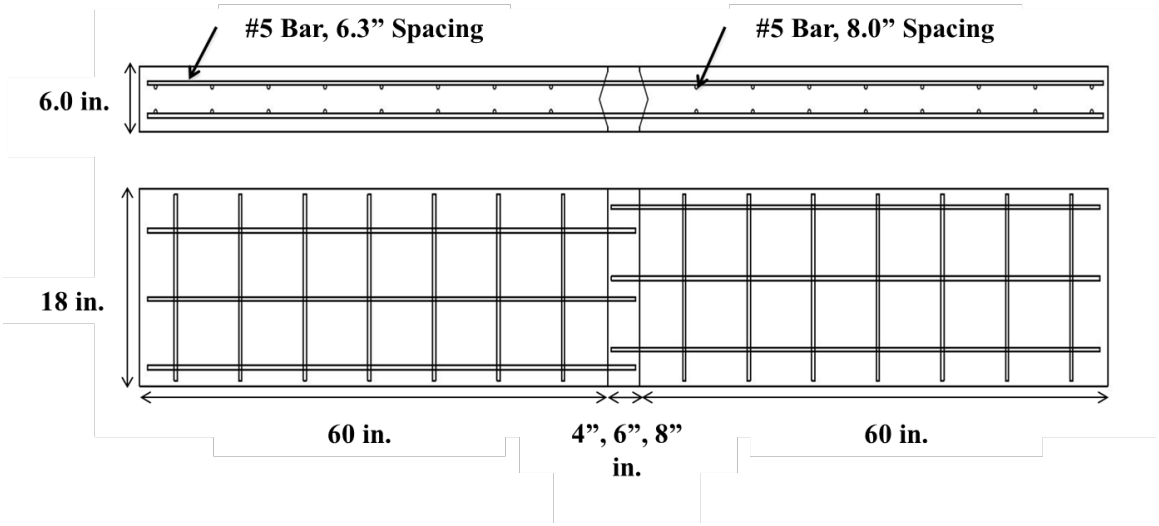

(a) Pure flexure specimens

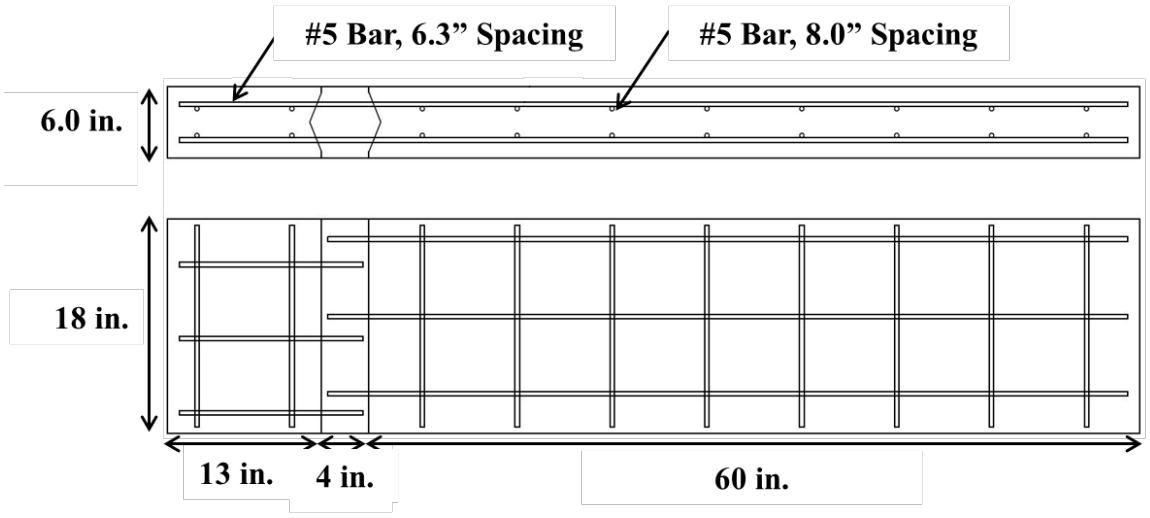

(b) Combined shear/flexure specimens

Figure 6-2: Joint Dimensions and Reinforcement Details

6.2.4. Specimens Tested and Material Parameters

Table 6-1 summarizes the main variables for the specimens tested in this study. The naming convention for the specimens is as follows: test type – joint width – fiber volume content – and test number. For example, an F-100-1P-1 mean the specimen was tested in pure flexure, with a 4" (100 mm) joint, containing 1.0% fiber volume content UHPC and was the first test in the series. All tests were performed after 28 days of concrete curing. Figure 6-2(a and b) provide a more detailed view of the lap spliced joint used for this study. The joint features a shear key design, minimizing the joint at the opening, expanding slightly in the center. This increased width at mid-depth enables an increased splice length while maintaining a small joint opening and minimizing total required volume of UHPC. Figure 6-2c shows the lap splice connection used for all of the specimens tested.

Name	Test Type	Lap Length, inches (mm) (Designed)	Lap Length, inches (Constructed)	Fiber Volume Content (%)	Inter-bar Spacing, inches	Fc' (ksi)
F-100-1P-1	Flexure	4" (100.0)	3.9	1.0%	6.3	26.1
F-100-1P-2	Flexure	4" (100.0)	3.8	1.0%	6.3	26.1
F-100-2P-1	Flexure	4" (100.0)	3.9	2.0%	6.3	27.7
F-100-2P-2	Flexure	4" (100.0)	3.9	2.0%	6.3	27.7
F-150-2P-1	Flexure	6" (150.0)	6.0	2.0%	6.3	27.7
F-150-2P-2	Flexure	6" (150.0)	5.3	2.0%	6.3	27.7
F-200-2P-1	Flexure	8" (200.0)	7.4	2.0%	6.3	27.7
F-200-2P-2	Flexure	8" (200.0)	7.5	2.0%	6.3	27.7
SF-100-1P-1	Combined	4" (100.0)	3.9	1.0%	6.3	26.1
SF-100-1P-2	Combined	4" (100.0)	3.9	1.0%	6.3	26.1
SF-100-2P-1	Combined	4" (100.0)	3.9	2.0%	6.3	27.7

Name	Test Type	Lap Length, inches (mm) (Designed)	Lap Length, inches (Constructed)	Fiber Volume Content (%)	Inter-bar Spacing, inches	Fc' (ksi)
SF-100-2P-2	Combined	4" (100.0)	3.8	2.0%	6.3	27.7

Table 6-1: Main Variable of Beam Specimens

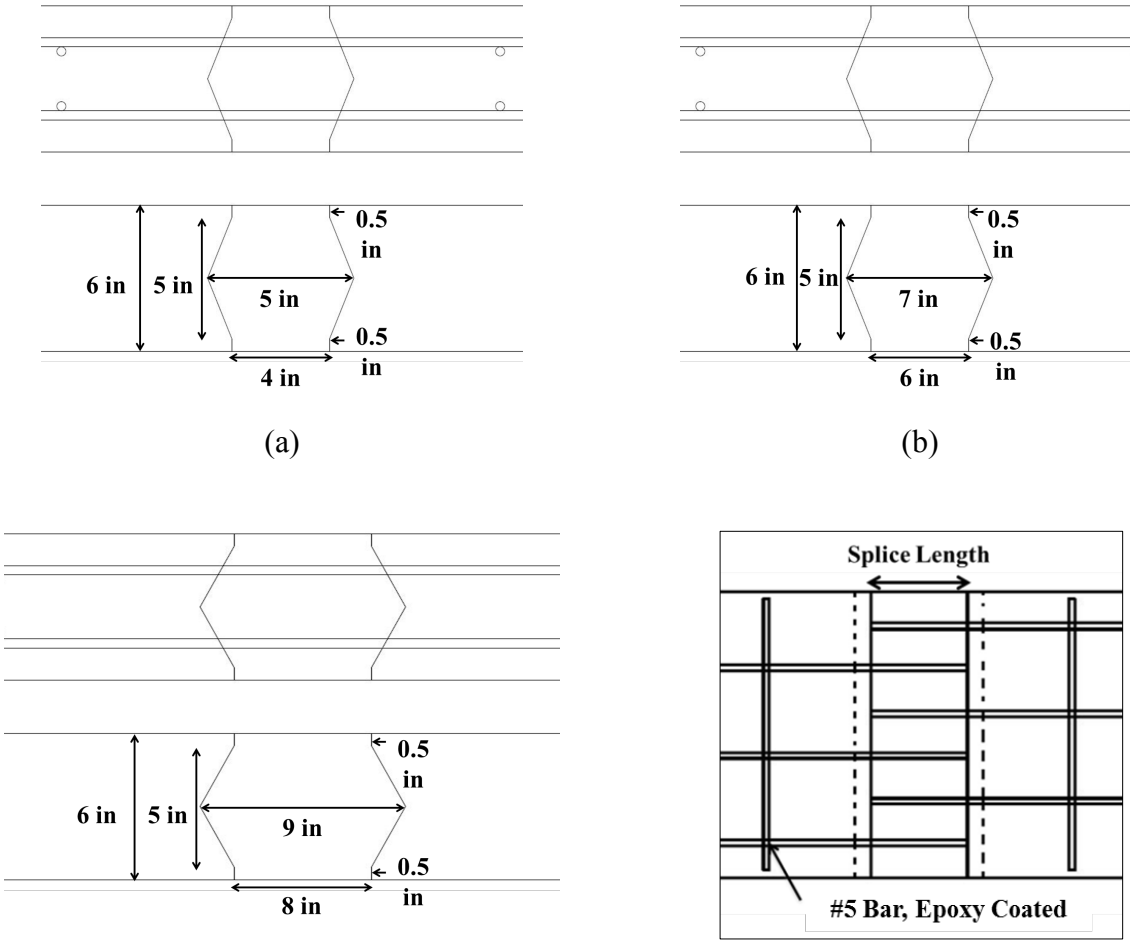

Figure 6-3 Joint Shape Details for the 4 in (a), 6 in (b) 8 in (c) joint, Lap Splice Connection Detail (d)

6.3. EXPERIMENTAL PROCEDURE

6.3.1. Test Set Up

All specimens were simply supported. Supports were placed 2" (50 mm) from either edge of the deck. Two rollers applied the load and were placed 12" (300 mm) from either edge of the joint in the pure flexure cases. A single roller was applied 4" (100 mm) from the joint interface in the combined shear and flexure case. Load was applied using a 100 kip INSTRON hydraulic loading machine. A displacement controlled load was applied quasi-statically at 0.001 in/sec (0.0254 mm/sec).

6.3.2. Instrumentation

Load was recorded using a 100 kip load cell integrated with the hydraulic machine. Displacements were measured at the locations shown in Figure 6-4a using the Optotrack measurement system. This system uses a set of cameras to track the relative displacements of the markers shown in three dimensions. Additionally, in each of the precast segments of the beam, for the F-100 and F-200 specimens, strain gauges were placed on the lower layer of reinforcing steel, 1" (25.4 mm) from the edge of the joint interface, Figure 6-4b.

Digital imagine correlation (DIC) was used in order to map the strain developing in the UHPC joint, Figure 6-4c. In DIC, random speckle patterns are applied to the surface of the concrete, being sure to cross the UHPC-Regular concrete joint interface. A high resolution, high frame rate, camera then records the surface of the concrete, specifically the speckles, at a fixed frame rate throughout the test procedure. These images are then uploaded, and the DIC software maps the locations and movements of the speckled pattern. Measuring the relative movements and

calculating displacements between the speckles allows for an accurate, 2-D, depiction of the strains occurring in the specimen, clearly highlighting crack patterns.

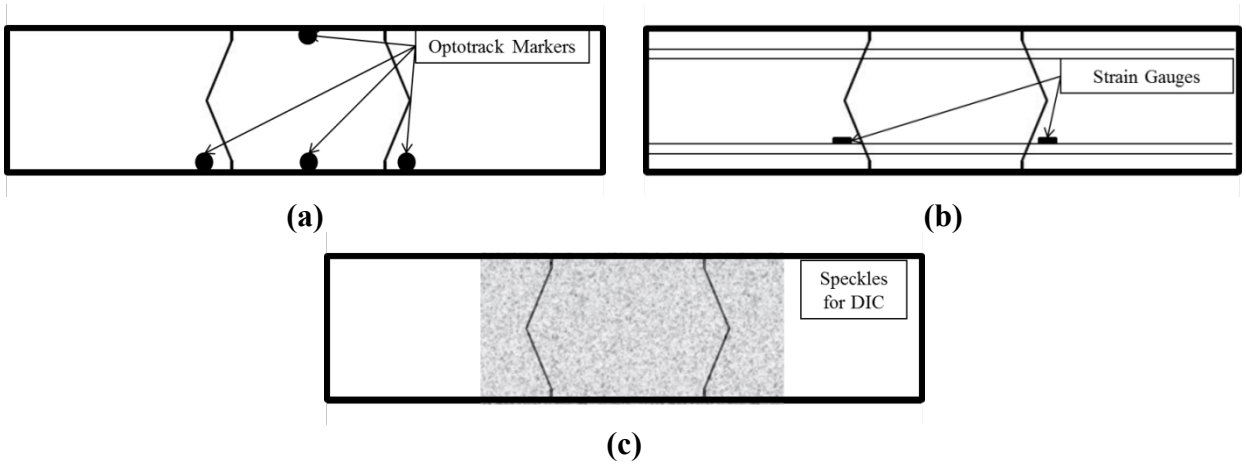

Figure 6-4: Instrumentation of the Precast Bridge Deck Beams

Data collected from the strain gauges placed on the deformed bars was used to verify the point during the test at which steel yielded. Data from the Optotrack system and DIC were used to measure deflections and strains occurring throughout the joint during testing. Data collected on the load and displacements were then plotted. The resulting curves were then processed through a moving average filter to account for minute changes due to the sensitivity of the equipment.

6.4. MATERIALS

The concrete used to construct the precast bridge deck elements consists of regular 5000 psi (35 MPa) concrete, with a 6” (150 mm) slump and maximum aggregate size of 0.78” (19 mm). The deformed bars all consisted of grade 60, epoxy coated steel and can be seen in Figure 6-5.

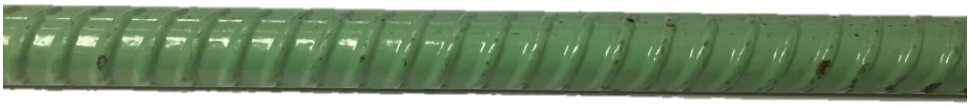

Figure 6-5: Deformed #5 (16 mm) Epoxy Reinforcement Bar

The UHPC mix design used to fill the joint and complete the lap splice follows the low-cost mix recommended in Chapter 3 (GG-25-00). The performance parameters for this mix can be found in Table 3-4.

6.5. CONSTRUCTION OF THE PRECAST CONCRETE SPECIMENS

Construction of the specimens for this study was performed in a simple, and easy to replicate process. Wood forms were first constructed with dimensions as designed. Once the rebar was placed, the shape of the joint's interface was created using a high-density foam and cut to the according dimensions (Figure 6-6b). Once the bars were in place and the bars were properly instrumented, the regular concrete was poured into the forms. Vibration was used to ensure proper installation of the regular concrete. After pouring, the surface of the concrete was smoothed and leveled so as to provide an adequate loading surface.

Twenty-four hours after the regular concrete had been cast; the foam was removed, exposing the inner surface of the joint. The two precast sections were brought together, and the splice properly aligned and measured. The bars were cleaned of any dirt and debris that had accumulated during the casting of the decks. The UHPC was then mixed and poured as described in Section 3.2.2. For this study, the UHPC was poured so as to favor fiber orientation in parallel to the deformed bars (Figure 6-6c). The specimens were then allowed to cure at room temperature for 28 days.

Following the prescribed curing time, the forms were removed and the speckles were painted onto the joint surface for the DIC measurements (Figure 6-6d).

(a)

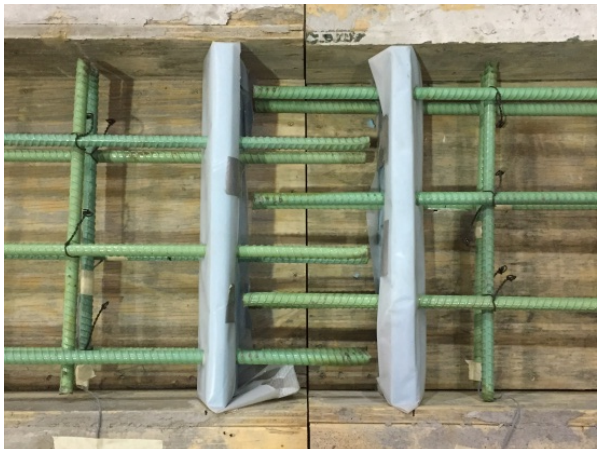

(b)

(c)

(d)

Figure 6-6: Forms and Placed Bars (a), Lap Splice (b), Poured UHPC Joint (c), and Set up with DIC (d)

6.6. RESULTS AND DISCUSSION

A summary of the results from the experimental testing for all of the specimens can be seen in Table 6-2.

Name	Embedded inches	Splice inches	Failure Mode	Force at Failure kips (Force/2)	Bond ksi
F-100-1P-1	4	3.5	Splitting	4.3	2.1
F-100-1P-2	4	3.5	Splitting	4.3	2.1
F-100-2P-1	4	3.5	Splitting	4.6	2.2
F-100-2P-2	4	3.5	Splitting	4.8	2.3
F-150-2P-1	6	5.9	Steel Yield	6.5	2.1
F-150-2P-2	6	5.8	Steel Yield	6.3	2.3
F-200-2P-1	8	7.8	Steel Yield	6.3	1.8
F-200-2P-2	8	7.8	Steel Yield	6.8	1.8
SF-100-1P-1	4	3.7	Splitting	15.2	2.1
SF-100-1P-2	4	3.9	Splitting	13.1	1.8
SF-100-2P-1	4	3.8	Splitting	16.3	2.2
SF-100-2P-2	4	3.8	Splitting	18.5	2.5

Table 6-2: Summary of Results from Experimental Testing

6.6.1. Comparison of Calculated Bar Stress versus Measured Bar Stress

Figure 6-7 shows the computed bar stresses calculated from the peak load recorded by the load cell compared to the measured strain (converted to stress) from the instrumented deformed bars. From the scatter, the calculated and measured data show no significant variation, though the calculated bar stresses generally measure slightly higher than those measured with the strain gauge. Thus the data is reliable and can be used for evaluation of the test data.

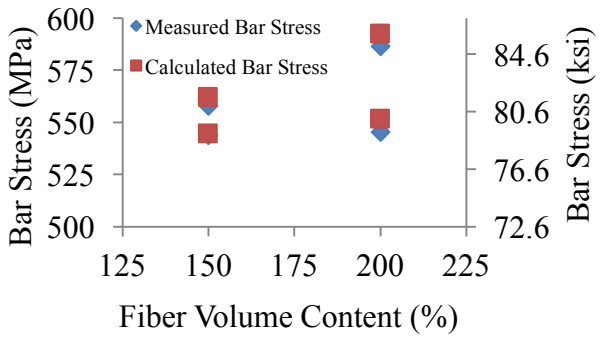

Figure 6-7: Comparison of Calculated and Measured Bar Stresses

6.6.2. F-100 Specimen Tests

Figure 6-8c and Figure 6-8d shows the force-displacement behavior of the four F-100 specimens subjected to flexural loading. For all tests, the load-displacement relation remained linear up to about 80% of the peak load. At this point, the load began to drop, corresponding to initial cracking at the center of the joint as can be seen by the horizontal cracks in Figure 6-8a and Figure 6-8b. The first crack to develop was the horizontal crack spanning the UHPC joint followed by a crack at the interface between the UHPC and regular concrete. For the rest of the loading, all deflections in the beam were localized at this interface. Figure 6-8a also shows the DIC images from the beams. As seen, all of the damage occurred in the joint, and that the corresponding crack pattern shows that a splitting failure occurred, where the reinforcement steel separated from the UHPC. No significant crushing in the regular concrete or UHPC was observed prior to the steel bar yielding. The peak force averaged 8.2 kips (36.5 KN) for specimens with 1% fibers (F-100-1P) by volume and 9.1 kips (40.5 KN) for those with 2% fibers (F-100-2P) by volume.

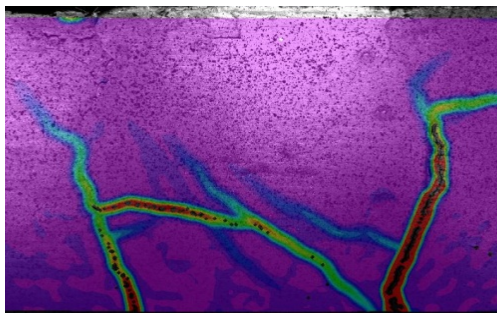

(a) **(b)**

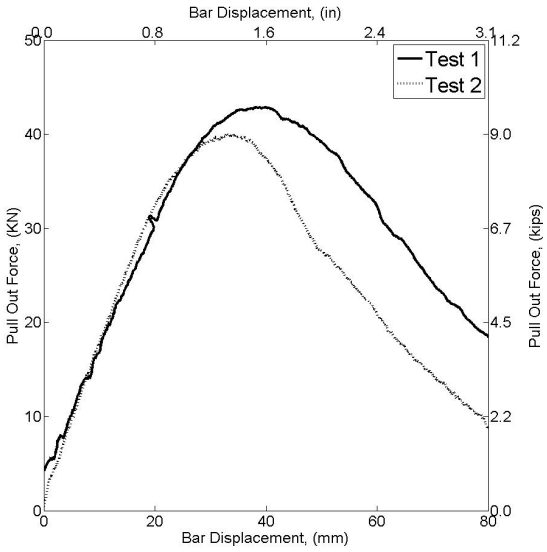

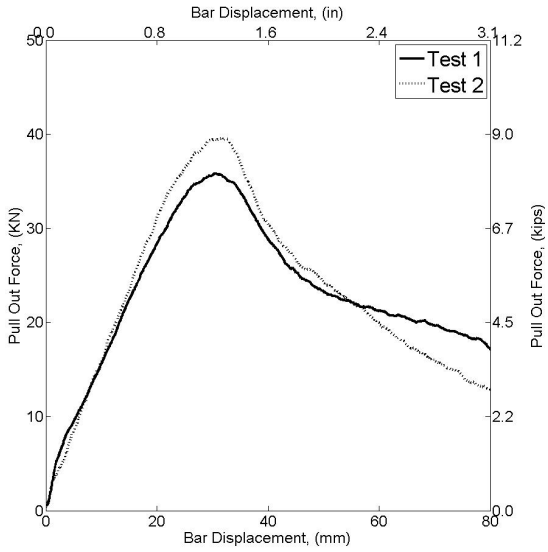

(c) **(d)**

Figure 6-8: (a) DIC of 100 mm joint specimens, (b) Splitting Failure in deformed specimen, (c) Load-Deflection Curves for 100 mm specimens with 2% fibers and (d) 100 mm specimens with 1% fibers.

6.6.3. F-150 and F-200 Specimens

Both F-150-2P and F-200-2P specimens were able to transfer the load in the joint past steel bar yield in the specimens. Figure 6-9c shows the load-displacement curve for both of the F-150-2P specimens tested. The load-deflection begins with an elastic increase in the load being applied. This is followed by a region of decreased slope in the load-deflection, caused by yielding of the steel reinforcement. As steel yielded, flexural cracking was observed in the regular concrete

regions of the deck. Load continues to climb until reaching a maximum average value of 13.3 kips (59.2 KN). At this point, a sudden crushing of the regular concrete at the UHPC joint interface occurs, observed in the load-deflection curve as the drop off in the load occurring at 2.55" (65 mm) of midspan deflection. At this point the beam was no longer able to carry additional load, and began to gradually drop towards zero. No damage was observed in the UHPC joint.

Figure 6-9d shows the load-displacement curve for both of the F-200-2P specimens tested. Similarly to the F-150-2P specimens, the load-deflection begins with an elastic increase in the load being applied. Again, this is followed by a region of decreased slope in the load-deflection, caused by yielding of the steel reinforcement. Flexural cracking in the regular concrete regions of the deck were also observed. Load continued to climb until reaching a maximum average value of 12.6 kips (56.0 KN). Again, at the point of maximum load, a sudden crushing of the regular concrete at the UHPC joint interface occurs, observed in the load-deflection curve as the drop off in the load occurring at 65 mm of mid-span deflection for F-200-2P-1 and 3.2" (80 mm) for F-200-2P-2. At this point the beams were no longer able to carry additional load, and began to gradually drop towards zero. As in the F-150-2P tests, no damage was observed in the UHPC joint.

Figure 6-9a shows the results from the DIC typical for both F-150-2P and F-200-2P specimens. The figure clearly shows that all of the deformation in the beam is occurring at the UHPC joint – regular concrete interface, and not across the joint itself as observed in the F-100 tests, confirming that the UHPC and steel reinforcement remained bonded throughout testing. Additionally, Figure 6-9b shows that the same lack of damage and cracking occurs on the other side of the beam, with small crack openings visible the UHPC-regular concrete interfaces.

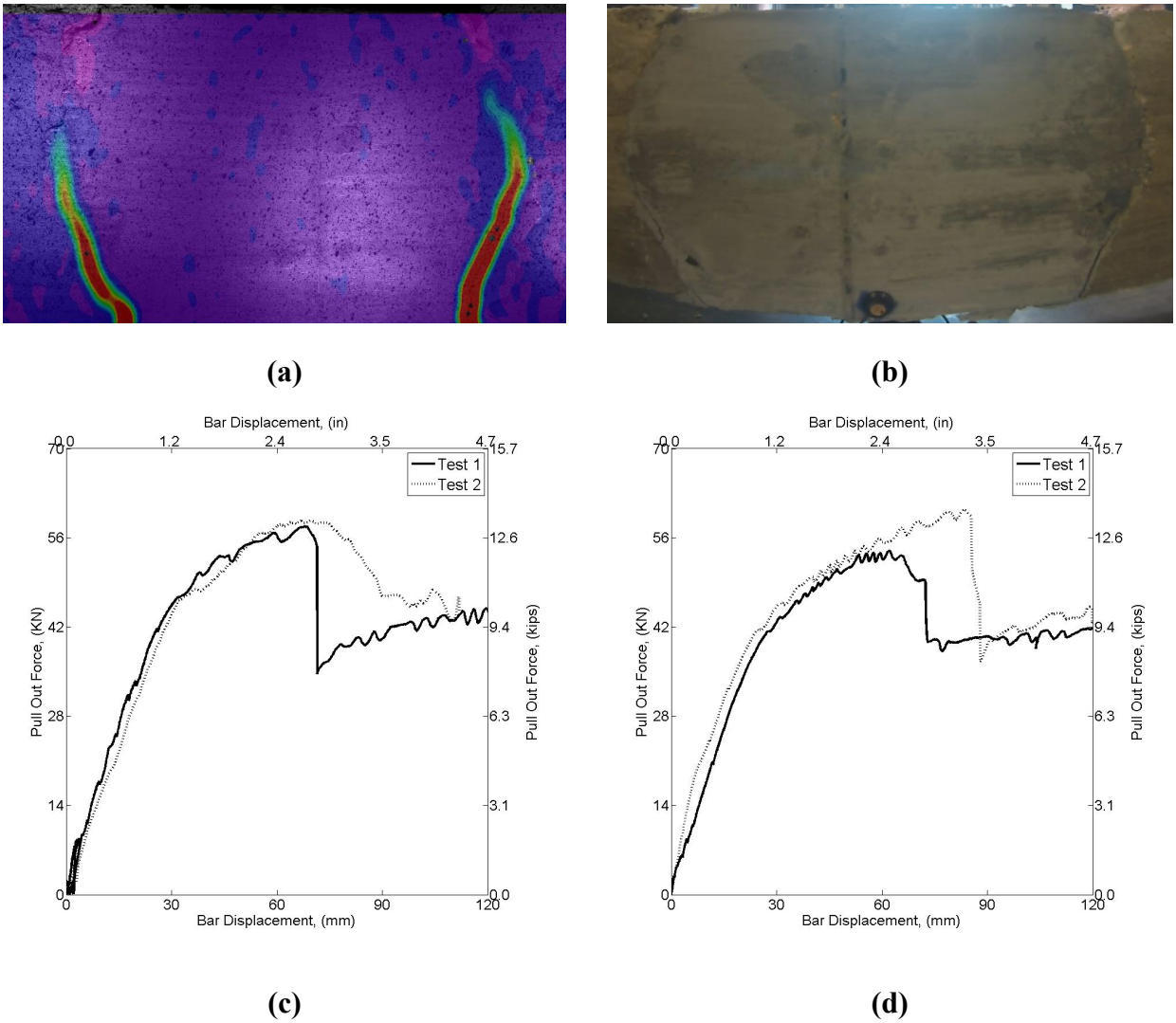

Figure 6-9: (a) DIC of 150 mm joint specimens, (b) Splitting Failure in deformed specimen, (c) Load-Deflection Curves for 150 mm specimens and (d) 200 mm specimens.

6.6.4. Effect of Fiber Content in Pure Flexure

As discussed in the previous sections, F-100-1P and F-100-2P specimens were both unable to successfully join the two precast regular concrete deck elements, resulting in a bar pull out failure to occur within the joint. The difference of 1% fibers by volume accounted for an average decrease in maximum force (and bond stress) of 8%. Cracked section calculations at the joint shows that at the point of maximum load, F-100-1P specimens experienced average bar force of 36.5 kips (162.3 KN) and F-100-2P specimens experienced an average bar stress of 40.5 kips

(180 KN). Figure 6-10 plots the maximum force reached for the two tests with respect to the fiber volume content of the UHPCs. Extrapolating from the existing data and assuming no problems with mix workability due to increased fiber content, a UHPC with a minimum fiber content of 3.5% would be required if using a 100 mm wide joint in order to successfully connect two pre-cast regular concrete elements. This represents an increase of 75% fibers versus F-100-2P specimens, and a 25% increase in fibers versus the F-150-2P. As previously discussed in chapter 3, fibers are the most costly components of UHPC, and thus the use of a wider joint width becomes more economical than the smaller joint with an increase in fibers.

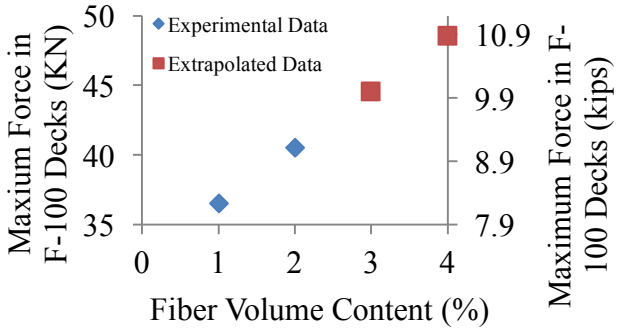

Figure 6-10: Maximum Force in F-100 Decks at a Function of Fiber Volume Content

6.6.5. Effect of Joint Size

Unlike F-100-1P and 2P specimens, both the F-150-2P and F-200-2P specimens were able to complete the joint connection. Figure 6-11 shows the moment (KN-m) at the joint as a function of the joint width for all tests with UHPC containing 2% fibers by volume. At 4" (100 mm), the maximum average moment achieved, 9 kip-ft. (12.2 KN-m), is the lowest. At 6" (150 mm) the average maximum moment achieved is 12.4 kip-ft. (16.9 KN-m) and 13.2 kip-ft. (17.8 KN-m) at 8" (200 mm). The increased width of 50 mm (a 34% increase in width and subsequently,

quantity of UHPC needed) between the F-150 and F-200 specimens only achieved an increase in moment capacity of 5.5%. In order to minimize required quantity of UHPC, the F-150-2P joints would provide the best UHPC use – beam strength ratio, despite the marginal gain in moment capacity.

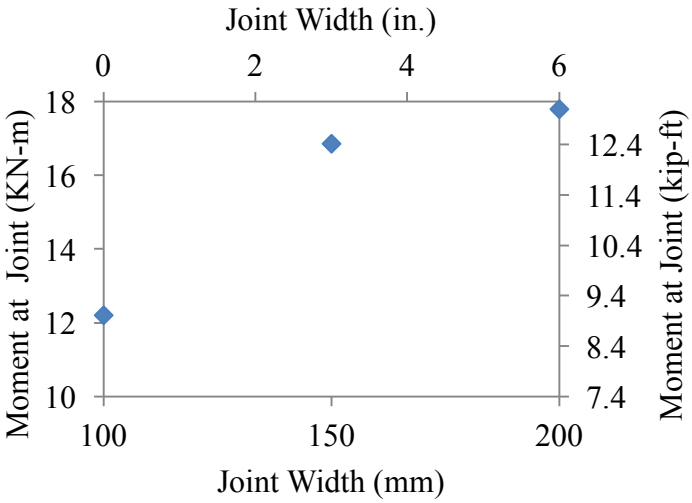

Figure 6-11: Moment at Joint as a function of Joint Width

6.6.6. Combined Shear and Flexure Testing

For the SF-100-1P specimens the load-displacement curve remained linear up to about 95% of the peak load. At this point, the load began to drop, corresponding to initial cracking at the center of the joint as can be seen by the horizontal cracks in Figure 6-12a and Figure 6-12b. The first crack to develop was the horizontal crack spanning the UHPC joint followed by a crack at the interface between the UHPC and regular concrete. For the rest of the loading, all deflections in the beam were at this interface. Figure 6-12a also shows the DIC images from the beams. Similarly to the F-100-1P and F-100-2P specimens, all of the damage occurred in the joint, and that the corresponding crack pattern shows that a splitting failure occurred, where the

reinforcement steel separated from the UHPC. No significant crushing in the regular concrete or UHPC was observed prior to the steel bar yielding. The peak force averaged 13.7 kips (61 KN) for specimens with 1% fibers (SF-100-1P) by volume and 16.9 (75.5 KN) for those with 2% fibers (SF-100-2P) by volume. Damage showed in Figure 6-12a and Figure 6-12b were representative for SF-100-1P-1, 2 and SF-100-2P-2. For SF-100-2P-1, the concrete between the UHPC joint and the closest support experienced a splitting crack, reducing the overall force achieved in the beam. This event can be seen as the sudden drop off in force on the load displacement curve.

6.6.7. Effect of Fiber Content in Combined Shear and Flexure

On average, SF-100-1P specimens containing 1% fibers by volume achieved 19% less force prior to failure than their SF-100-2P counterparts. This result is unsurprising as bonding in UHPC is directly related to the steel fiber contents, as discussed in Chapter 5. SF specimens containing 1% steel fibers by volume averaged 8% less bar force at failure that their pure flexure counterpart with 1% fibers by volume. At 2% fibers by volume, the difference in bar forces achieved between F-100-2P and SF-100-2P specimens was less pronounced, suggesting that the UHPC's capacity in shear increases non-linearly with increases with fiber content. More testing on UHPC specimens in shear should be conducted in order to further clarify these results.

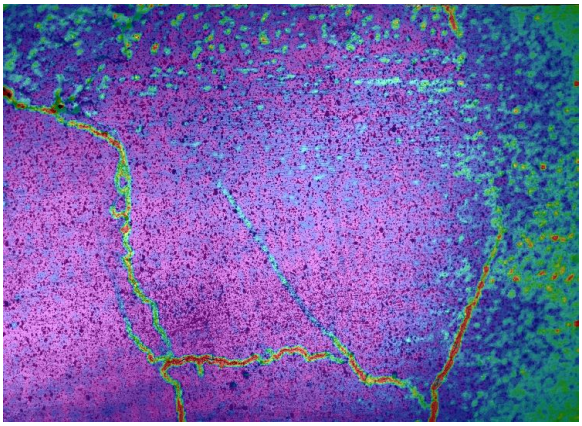

(a)

(b)

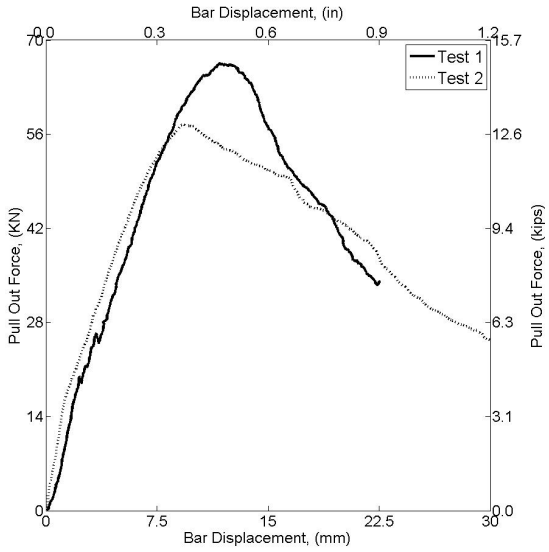

(c)

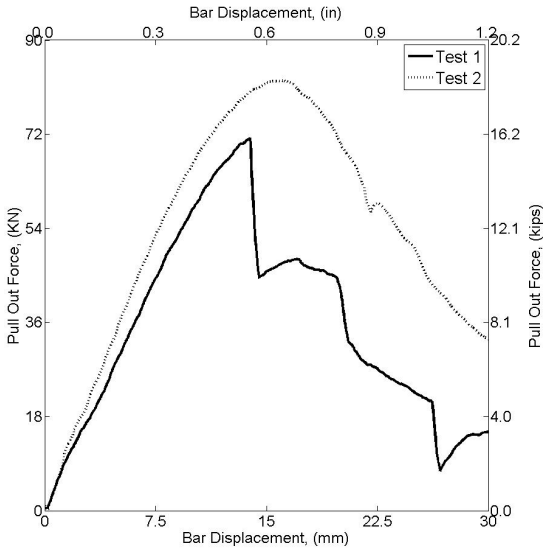

(d)

Figure 6-12: (a) DIC of 100 mm joint, SF specimens, (b) Splitting Failure in deformed specimen, (c) Load-Deflection Curves for 100 mm specimens, 1% fiber by vol. and (d) 100 mm specimens, 2% fiber by vol.

6.7. FINITE ELEMENT MODEL AND PARAMETRIC STUDY

6.7.1. Model Setup

A two dimensional finite element model was developed for the LS-DYNA platform. The model makes use of 2-D plane stress elements. The model was discretized and meshed using

Hypermesh, and can be seen in Figure 6-13. Each model consists of three components; 2 precast regular concrete elements and 1 UHPC joint. Specimen dimensions and reinforcement details follow those prescribed previously for the F-150-2P and F-200-2P specimens.

Reinforcing steel was modeled using one dimensional, linear beam elements. The steel bars and surrounding concrete were assumed to be perfectly bonded. As only reinforcing steel from the F-150-1P and F-200-2P specimens remained fully bonded, only those two specimens were used in this portion of the study.

Steel material behavior was modeled using a piecewise linear plasticity model (LS-DYNA card #24). Steel material properties were determined through experimental testing, with the following parameters: yield stress, σ_y = 67 ksi (450 MPa) with a young's modulus, E = 29000 ksi (200 GPa). After yield, the tangent modulus E_{tan} was set to 175 ksi (1.2 GPa). Figure 6-12 shows the finite element model (a) and mesh (b) developed for use in this study for the F-150-2P specimens (at 6").

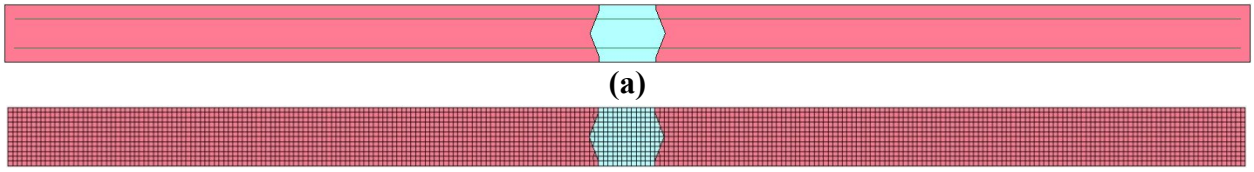

Figure 6-13: (a) Finite Element Model and (b) Mesh for F-150-2P Specimens

6.7.2. UHPC and Concrete Material Models

The concrete material model used in this study was previously developed model for high performance fiber reinforced composites (Hung, 2010), and calibrated for use with UHPC based on the experimental results previously reported. The model, based upon a hybrid rotating/fixed

crack approach, allows perpendicular cracking of the concrete and is capable of modeling the tensile and compressive response for UHPC. The tensile response is characterized by three regions, a linear elastic portion followed by some strain hardening and then a softening of the concrete. Figure 6-14a shows the typical tensile response of uniaxial testing on UHPC specimens as well the material model response used in this study. Figure 6-14b shows the compressive response of UHPC under loading experimentally as well as the model's material response. For the regular concrete material, the same hybrid rotating/fixed crack model was employed, calibrating it with typical concrete responses. Table 6-3 outlines the material properties used.

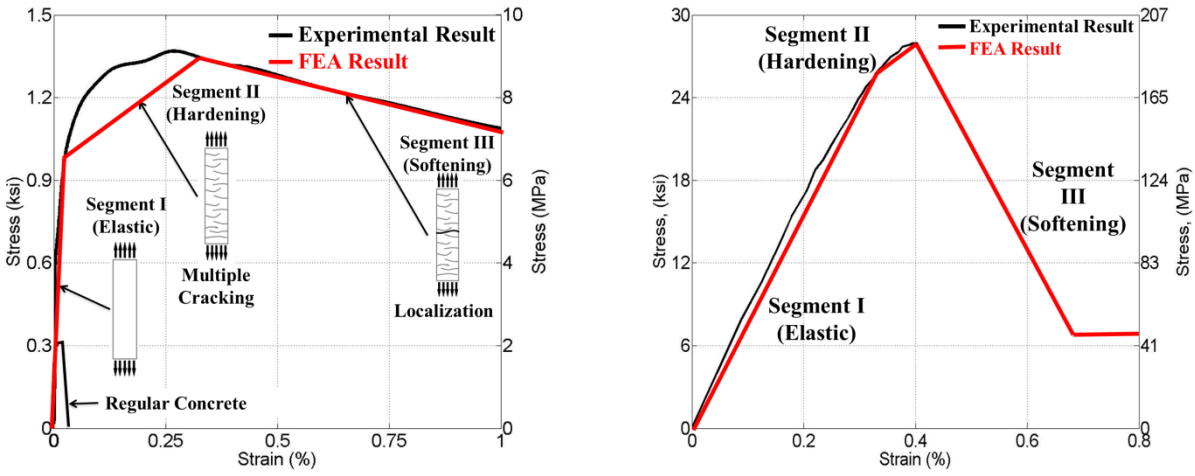

(a) (b)

Figure 6-14: Typical UHPC Tensile Response for Joint Fill Material (a) tension and (b) compression

Name	Tensile Pre-Cracking Stress (Strain)	Tensile Post-Cracking Stress (Strain)	Elastic Modulus	F'c (ksi)
UHPC	0.75 ksi (0.0001)	1.2 ksi (0.0002)	751 ksi	26.8
Regular Concrete	0.35 ksi (0.0001)	0.01 ksi (0.0002)	157 ksi	5.0

Table 6-3: Material Parameters for FEM

6.7.3. Parametric Study

The finite element model was validated using the experimental data and from there, a parametric study was performed to determine the effect of the joint's surface topology on the overall performance of the beams. Three different joint designs were modeled and analyzed and can be seen in Figure 6-15. For each joint type, modeling was performed for a 6" (150 mm) joint as well as an 8" (200 mm) joint. Figure 6-15a shows the original joint design tested experimentally and used for the model validation (F-150-2P). Figure 6-15b shows a non-tapered (NT) joint design, and Figure 6-15c shows the flat surface (FS) joint design modeled for the parametric study. The NT and FS joint designs were selected, as they both are more easily constructed designs. A summary of the simulations performed can be found in Table 6-4.

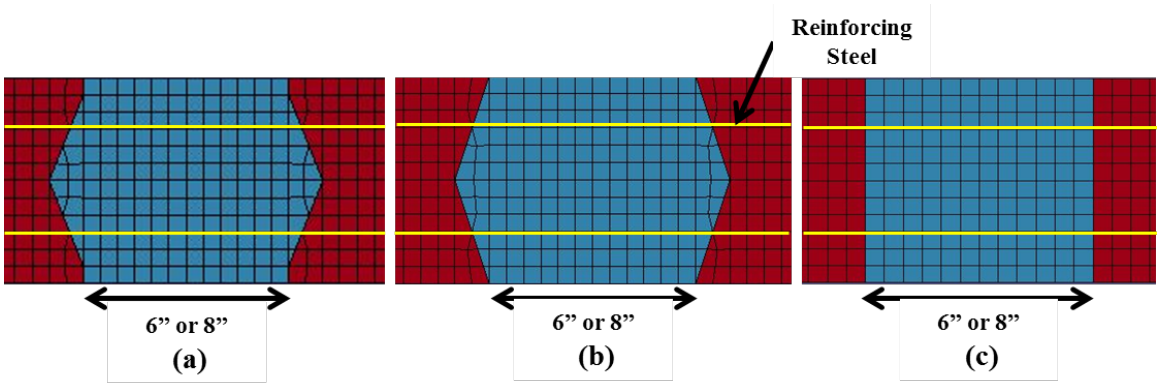

Figure 6-15: (a) Original Joint Design for FEA, (b) non-tapered joint design, and (c) flat joint design.

Name	Joint Type	Joint Size inches (mm)
F-150	Flexure (as F-150-2P)	6” (150)
NT-150	Non-Tapered	6” (150)
FS-150	Flat Surface	6” (150)
F-200	Flexure (as F-200-2P)	8” (200)
NT-200	Non-Tapered	8” (200)
FS-200	Flat Surface	8” (200)

Table 6-4: Summary of Simulated Beams

6.7.4. Model Validation

Results from the experimental testing of beams F-150-2P and F-200-2P were used for model validation. From Figure 6-16a, the numerical results (red line) show good correlation with the results from the experimental testing (black line), including capturing the steel yield, and later on the concrete crushing which occurs for the F-150-2P specimens. Additionally, the deformed shape matches well with the observed experimental deformations (Figure 6-17). While some discrepancies exist, the values from the simulation match reasonably well with the experimental values, and the minor discrepancies between the simulation and experimental data are attributed to experimental scatter. The same conclusion can be reached for the results of the F-200-2P model validation seen in Figure 6-16b.

6.7.5. Results of Parametric Study

For the 150 mm joints, the results from the FEA showed little variation between the F-150, NT-150 and FS-150 joints. All three load-displacement curves began elastically, up until 80% of their max load, at which point the steel reinforcement began to yield. Yielding continued, with the load increasing until approximately 65 mm midpoint deflection. At this point, the concrete at

the top of the UHPC-regular concrete interface was crushed, resulting in a drop off in the force capacity of the beam. There was no noticeable difference between the F, NT and FS joints.

Similarly, the F-200, NT-200 and FS-150 joints show little variation. Again, all three load-displacement curves began elastically, up until 80% of their max load, at which point the steel reinforcement began to yield. Yielding continued, with the load increasing until approximately 70 mm midpoint deflection. At this point, the concrete at the top of the UHPC-regular concrete interface was crushed, resulting in a drop off in the force capacity of the beam.

As these simulations were performed under pure flexure for all three joint types, their respective topologies were not fully engaged leading to the primarily flexure failure mechanism. In a more realistic scenario, the shear strength of the UHPC at the joint interface would become important, as more joints are not solely subjected to flexure. Results from the combined shear and flexure testing could not be used for model validation as the primary failure modes in those tests was a bar pull out failure in the joint and thus, a parametric study could not be done for the combined shear and flexure case. UHPC specimens under shear should be further studied to gain more insight into the behavior.

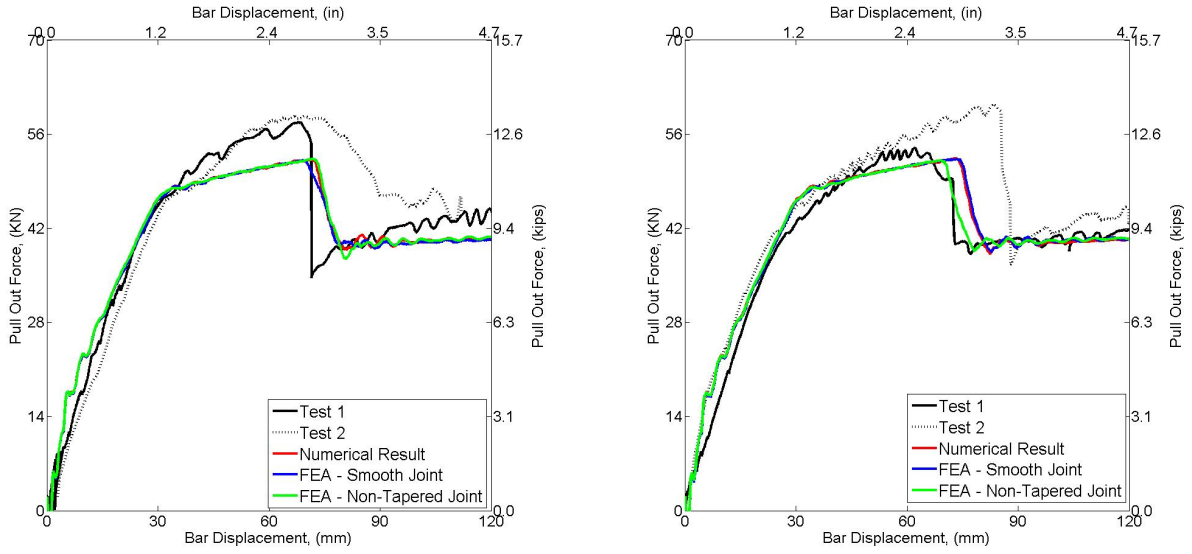

Figure 6-16: Experimental FEA Load-Deflection for (a) 150 mm joints and (b) 200 mm joints

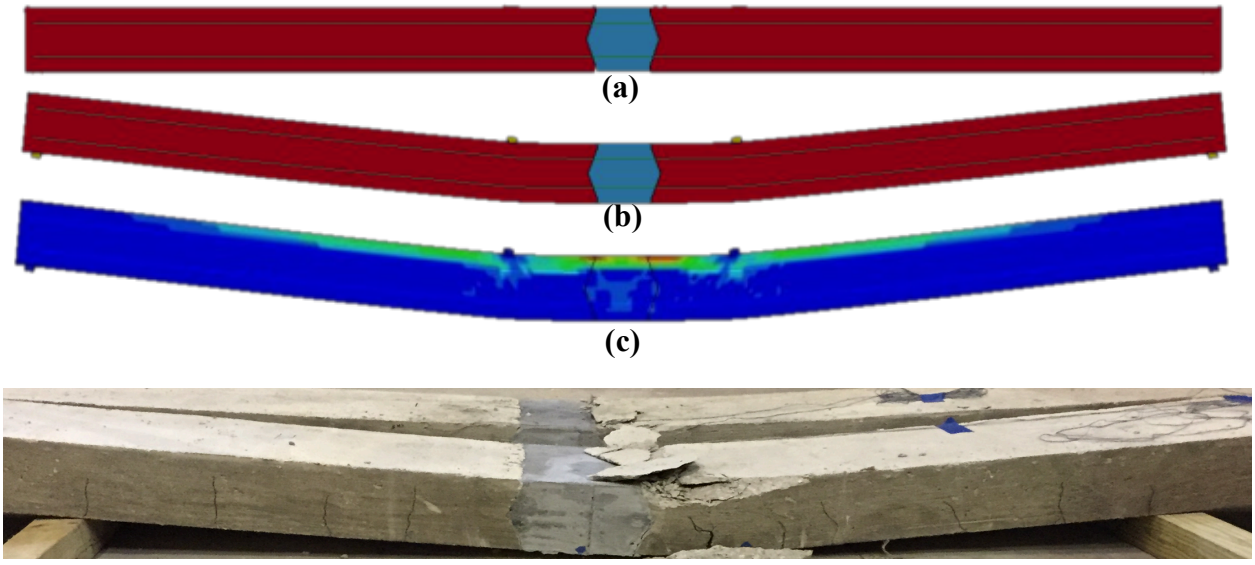

Figure 6-17: (a) Un-deformed shape, (b) deformed shape and (c) von Mises Strain for 150 mm, (d) Plot of the cracks developed and (e) and Damaged Beam after Testing, Actual joint

6.8. CONCLUSION

The objective of the study in this chapter was to evaluate the use of ultra-high performance concrete for simplified joint connections between precast bridge deck elements. The study evaluated three different joint widths, two different fiber volume content UHPCs and two separate loading schemes to simulate real-world loading conditions. The conclusions are as follow:

- All F-100 and SF-100 (4" joint) specimens failed with a splitting failure occurring at the UHPC joints. Bond between the UHPC and deformed bars was insufficient, causing the beams to reach failure prematurely.
- F-150 and F-200 (6" and 8" joints) specimens all failed through steel yield in the deformed bars, followed much later on by crushing in the regular concrete. These specimens were able to carry load through the joints all the way through the desired failure mode.
- F-100 (4" joint) specimens containing 1% fibers by volume achieved an average of 8% lower capacity (and hence bond stress in the joints) than those containing 2% fibers. Extrapolating the test results suggests that a 4" (100 mm) joint may be possible when utilizing a greater steel fiber ratio (~3%). However, increased fiber content leads to greater cost and, possibly, problems with mix workability. Mixes with such high fiber contents were not tested in this work.
- SF-100 (4" joint) beams performed worse than F-100 beams at 1% fibers by volume, though the difference at 2% fibers by volume was non-apparent. This suggests the increase in shear strength in UHPC increases non-linearly with an increase in steel fiber content compared to flexure strength and should be investigated further.

- Changes in the topology of the joint showed no difference in structural performance in the parametric study, under pure flexural loading.

Intentionally left blank

7. SUMMARY, MAJOR CONCLUSIONS AND FUTURE RESEARCH

7.1. SUMMARY AND MAJOR CONCLUSIONS

The primary objectives of this project were: 1) to develop a cost-optimized version of non-proprietary UHPC and characterize its mechanical and durability properties, and 2) investigate the possibility of using UHPC for field-cast joints that commonly occur in precast construction. To achieve these objectives, the first phase of the work looked into the material components of non-proprietary UHPC, and through an analysis of their costs, quantities, and availabilities, a new low-cost alternative UHPC mix formulation was designed. The material cost of this alternative mix is half of the original UHPC mix. Using the new alternative low cost mix, and a select few seen as reduced cost alternatives, a detailed investigation of their mechanical and durability properties was conducted. Mechanical property characterization focused on quantifying tensile properties and compressive strength, while durability studies addressed the material's air voids, resistance to freeze-thaw and chloride penetration. All tested mixes had exceptional mechanical and durability properties.

The proposed mix deviates from traditional UHPC mixtures in that it uses a 50:50 mix of Portland Type I and Ground Granulated Blast Furnace Slag (GGBS) as a binder, lacks any Silica Powder (inert filler) and requires no post-placing treatment. The use of GGBS improves the material's 'greenness' making it a more sustainable cementitious product. Specifications for making the new UHPC were proposed.

UHPC derives its unique properties from its high packing density, which is achieved by carefully controlling the size and distribution of the constituent particles, and incorporating steel fibers. For example, unlike regular concrete which relies on having sufficient void space to allow water

to expand, the high freeze-thaw resistance in UHPCs is due to water being prevented from entering the material in the first place.

The test results suggest that fiber volume contents of 1.0% or 1.5% could significantly reduce the chance for crack localization under dead load or working conditions, respectively, in structural applications. Coupled with the material's inherent resistance to chloride ion penetration, controlling crack localization further limits the ingress of chloride ions and protects steel reinforcement from corrosion.

Following material characterization, the next phase of the research investigated the bonding performance between steel reinforcement and UHPC. The study spanned several experimental parameters (embedment, bar size & type, UHPC fiber content/orientation, etc.), and ultimately led to a design guideline for achieving specific bar stresses when reinforcement is embedded in UHPC. This was then followed by a series of beam tests using two precast regular concrete sections joined together with a UHPC joint. The results of this testing showed that a 150 mm (6") UHPC was sufficient for precast bridge construction.

7.2. PROMISE AND COMMERCIAL POTENTIAL OF UHPC

The non-proprietary UHPC developed in this work has strong potential for use in structures that will be significantly more durable than currently possible with conventional materials. Therefore, every structure built at the moment using current technology is an opportunity lost to start building a longer lasting infrastructure that is considerably cheaper to maintain in the long run.

The current cost of a cubic yard of the nonproprietary UHPC developed in this work is $\$267/yd^3$ for the cementitious material alone. The addition of fibers at 1.5% by volume would enable the use of UHPC for structural applications, while minimizing the fiber cost. Each cubic yard of

UHPC requires 193 lbs. of steel fibers. Ordering from a supplier within the United States currently costs $1.98 per pound. Adding this $382/yd^3 fibers cost to the base $267/yd^3 brings the total cost to $659/yd^3, roughly 5x the present cost of regular concrete.

Several suppliers outside of the United States produce steel fibers at a reduced unit cost, as low as $0.30 per pound (e.g. http://tinyurl.com/h474res, accessed on 12/30/2015). Using these suppliers, and assuming that the fiber quality is similar to the US products, will reduce the current cost of UHPC (including fibers) to $325 per cubic yard, which is only about twice the cost of regular concrete.

7.3. AN OPPORTUNITY FOR THE STATE OF MICHIGAN

One of the reasons for the high US fiber costs is the lack of demand. As UHPC usage increases and demand for steel fibers surges, it is expected that the cost will drop. The State of Michigan, with its focus on vehicle manufacturing, is well suited to be major fiber industry hub given that steel fibers are made from chopped high strength wires that are used in steel-belted tire products.

7.4. A BRIGHT FUTURE

For an initial increase in material cost compared to regular concrete, whether 2x or even 5x, the benefits of UHPC can be substantial compared to traditional concrete products. With UHPC's enhanced strength in tension and compression, thinner and more elegant structures can be built. Not only that, the use of GGBS in the proposed mix improves the material's 'greenness' making it a more sustainable cementitious product. With durability that boasts no deterioration after 60+ cycles of freeze-thaw and virtually no chloride penetration, UHPC structures will have extremely

low maintenance requirements, and therefore costs, for lifespans that are substantially longer than currently possible.

7.5. FUTURE RESEARCH NEEDS

To achieve the promise of UHPC as the material for the next generation of infrastructure, research is needed on multiple fronts. Fibers properties need to be optimized and the effect of fiber coatings on UHPC response explored. Commercial production of UHPC remains a challenge. At present, UHPC must be mixed in a paddle mixer and cannot be made and delivered in a ready-mix concrete truck. Research is needed to explore innovative mixing methods that require only small incremental changes to existing mixing technology so that widespread adoption of the material can be facilitated. Research into alternative high range water reducers is also needed so as to ensure that the UHPC described herein is not dependent on a single source. Also, research on UHPC structures and structural components is rare in the literature and research efforts are needed to ensure that established design methods apply to UHPC systems and develop new ones, as needed.

8. REFERENCES

AASHTO T 132-87. Standard Method of Test for Tensile Strength of Hydraulic Cement Mortars. American Association of State and Highway Transportation Officials. 8 pages. 2009.

AASHTO T 277-86, Rapid Determination of the Chloride Permeability of Concrete, American Association of States Highway and Transportation Officials, Standard Specifications - Part II Tests, Washington, D. C., 1990.

ACI Committee 318-05 (2005). Building Code Requirements for Structural Concrete (ACI 318-05) and Commentary (ACI 318R-05), American Concrete Institute Committee 318, Farmington Hills, MI.

ACI Committee 408 (2003). Bond and Development of Straight Reinforcing Bars in Tension. ACI 408R-03, American Concrete Institute Committee 408, Farmington Hills, MI.

Acker, P. and Behloul, M., "Ductal® Technology: A Large Spectrum of Properties, A Wide Range of Applications," Proceedings of the International Symposium on Ultra High Performance Concrete, Ed., Schmidt, M., Fehling, E., and Geisenhanslüke, C., Kassel University Press, Kassel, Germany, 2004, pp. 11–23.

Ahlborn, T.M. et al., "Durability and Strength Characterization of Ultra-High Performance Concrete Under Variable Curing Regimes," Proceedings of the Second International Symposium on Ultra High Performance Concrete, Ed., Fehling, E., Schmidt, M., and Stürwald, S., Kassel University Press, Kassel, Germany, 2008, pp. 197–204.

Ahlbourn, Theresa. "ULTRA-HIGH PERFORMANCE CONCRETE FOR MICHIGAN BRIDGES." Final Report, MDOT, Michigan Tech (2008): 1-152. Web.

Alexander, M.g, and B.j Magee. "Durability Performance of Concrete Containing Condensed Silica Fume." Cement and Concrete Research 29.6 (1999): 917-22. Web.

Alkaysi, M., El-Tawil, S., Liu, Z. and Hansen, W. (2016), "Effects of Silica Powder and Cement Type on Long Term Durability of Ultra High Performance Concrete (UHPC)," Accepted for Publication in the ACI Materials Journal.

Andreasen, A.H.M. and Andersen, J., 'Ueber die Beziehung zwischen Kornabstufung und Zwischenraum in Produkten aus losen Körnern (mit einigen Experimenten)', Kolloid-Zeitschrift 50 (1930) 217-228.

Andreassen and J. Andersen: Kolloid Z. 50 (1930) p. 217–228.

ASCE 7: Minimum Design Loads for Buildings and Other Structures. N.p.: ASCE Library, n.d. Print.

ASTM Standard C109, Standard Test Method for Compressive Strength of Hydraulic Cement Mortars (Using 2-in. or (50-mm) Cube Specimens)', ASTM International, West Conshohocken, PA. (2009)

ASTM Standard C1202, "Standard Test Method for Electrical Indication of Concrete's Ability to Resist Chloride Ion Penetration", ASTM International, West Conshohocken, PA. (2009) 6 pp.

ASTM Standard C457, 'Standard test method for microscopical determination of parameters of the air-void system in hardened concrete', ASTM International, West Conshohocken, PA. (2009) 14 pp

Azizinamini, A., Stark, M., Toller, J.J., and Ghosh, S.K., 1993, "Bond Performance of Reinforcing Bars Embedded in High-Strength Concrete," ACI Structural Journal, V. 90, No. 5, Sep.-Cot., pp. 554-561.

Bonneau, O. et al., "Mechanical Properties and Durability of Two Industrial Reactive Powder Concretes," ACI Materials Journal, Vol. 94, No. 4, July–August 1997, pp. 286–290

Borges, Paulo H. R., Lucas F. Fonseca, Vitor A. Nunes, Tulio H. Panzera, and Carolina C Martuscelli. "Andreasen Particle Packing Method on the Development of Geopolymer Concrete for Civil Engineering." Journal of Materials in Civil Engineering (2013): 130413134609008. Web.

Brouwers HJH, Radix HJ, Self-compacting concrete: the role of the particle size distribution. In: The first international symposium on design, performance and use of self-consolidating concrete (SCC'2005) Changsha, Hunan, China; p. 109–18. 200

Castro, A. L., and Pandolfelli, V. C. (2009). "Review: Concepts of particle dispersion and packing for special concretes production." Cerâmica, 55(333), 18–32

Cheng, An, Ran Huang, Jiann-Kuo Wu, and Cheng-Hsin Chen. "Influence of GGBS on Durability and Corrosion Behavior of Reinforced Concrete." Materials Chemistry and Physics 93.2-3 (2005): 404-11. Web

Cheng, An, Ran Huang, Jiann-Kuo Wu, and Cheng-Hsin Chen. "Influence of GGBS on Durability and Corrosion Behavior of Reinforced Concrete." Materials Chemistry and Physics 93.2-3 (2005): 404-11. Web.

de Larrard, F. and Sedran, T., "Optimization of Ultra-High-Performance Concrete by the Use of a Packing Model," Cement and Concrete Research, Vol. 24, No. 6, 1994, pp. 997–1,009.

Elaty, Metwally Abd Allah Abd. "Compressive Strength Prediction of Portland Cement Concrete with Age Using a New Model." HBRC Journal 10.2 (2014): 145-55. Web.

Fehling, E., Lorenz, P., and Leutbecher, T., "Experimental Investigations on Anchorage of Rebars in UHPC," Proceedings of Hipermat 2012 3rd International Symposium on UHPC and Nanotechnology for High Performance Construction Materials, Ed., Schmidt, M.,Fehling, E.

Gilkey, Hj. "Bond with Reinforcing Steel." Significance of Tests and Properties of Concrete and Concrete Aggregates (1956): n. pag. Web.

Glotzbach, C., Fröhlich, S., and Piotrowski, S., Kassel University Press, Kassel,Germany, 2012, pp. 533–540.

Graybeal, B., "Behavior of Field-Cast Ultra-High Performance Concrete Bridge Deck Connections Under Cyclic and Static Structural Loading," FHWA, U.S. Department of Transportation, Report No. FHWA-HRT-11-023, National Technical Information ServiceAccession No. PB2011-101995, 2010.

Graybeal, B., "Bond Behavior of Reinforcing Steel in Ultra High Performance Concrete," Federal Highway Administration, FHWA-HRT-14-089, October, 2014, p. 12

Graybeal, B., "Design and Construction of Field-Cast UHPC Connnections," Federal Highway Administration, FHWA-HRT-14-084, October, 2014, p. 36

Graybeal, B., "Material Property Characterization of Ultra-High Performance Concrete," FHWA, U.S. Department of Transportation, Report No. FHWA-HRT-06-103, McLean, VA, 2006

Graybeal, B., Perry, V., and Royce, M., “UHPC Ultra-High Performance Concrete,” NHI Innovations Webinar, November 18, 2010. Available at https://connectdot.connectsolutions.com/n134083201011 (Cited April 3, 2012).

Graybeal, B.A. and Hartmann, J.L., “Strength and Durability of Ultra-High Performance Concrete,” Proceedings of the 3rd International Symposium on High Performance Concrete/PCI National Bridge Conference, October 19–22, 2003, Orlando, FL, Compact Disc, Paper 47.

Graybeal, Benjamin A. "Field-Cast UHPC Connections for Modular Bridge Deck Elements." FHWA-HRT-11-022 48.6 (2014): n. pag. FHWA. Web.

Graybeal, Benjamin A. "Splice Length of Prestressing Strands in Field-cast UHPC Connections." Mater Struct Materials and Structures 48.6 (2015): 1831-839. Web.

Graybeal. "Ultra-High Performance Concrete: A State-Of-The-Art Report for The Bridge Community." Chapters 6-7 - , June 2013 - FHWA-HRT-13-060. N.p., n.d. Web. 06 Dec. 2014.

Holschemacher, K. and Weiße, D., “Economic Mix Design Ultra High-Strength Concrete,” Seventh International Symposium on the Utilization of High-Strength/High-Performance Concrete, Vol. II, Publication No. SP-228, Ed., Russell, H.G., American Concrete Institute, Farmington Hills, MI, 2005, pp. 1,133–1,144.

Holschemacher, K., Weiβe, D., and Klotz, S., “Bond of Reinforcement in Ultra High Strength Concrete,” Proceedings of the International Symposium on Ultra High Performance Concrete, Ed., Schmidt, M., Fehling, E., and Geisenhanslüke, C., Kassel University Press, Kassel, Germany, 2004, pp. 375–387.

Hwang, Hoonhee, and Sung Yong Park. "A Study on the Flexural Behavior of Lap-spliced Cast-in-place Joints under Static Loading in Ultra-high Performance Concrete Bridge Deck Slabs." Canadian Journal of Civil Engineering Can. J. Civ. Eng. 41.7 (2014): 615-23. Web.

Innovative Field-Cast Uhpc Joints For Precast Bridge Decks - Highways for LIFE - FHWA."

Jungworth, J., Muttoni, A., "Structural Behavior of Tension Memebers in UHPC,"Proceedings of the International Symposium on Ultra High Performance Concrete, Kassel, Germany, 2004.

Kim, D-J., Wille, K., Naaman, A. E. and El-Tawil, S. (2011), "Strength Dependent Tensile Behavior of Strain Hardening Fiber Reinforced Concrete," Proceedings of HPFRCC6, H. W. Reinhardt and G. Parra Editors, Ann Arbor, MI.

Kim, D-J, Naaman, A. E. and El-Tawil, S. (2010a), "High Performance Fiber Reinforced Cement Composites With Innovative Slip Hardening Twisted Steel Fibers" International Journal of Concrete Structures and Materials, Korean Concrete Institute, ISSN: 1976-0485, 3(2), pp. 119 – 126; DOI 10.4334/IJCSM.2009.3.2.119.

Kim, D-J, El-Tawil, S., Sirijaroonchai, K. and Naaman, A. E. (2010b), "Numerical Simulation of the Split Hopkinson Pressure Bar Test Technique for Concrete Under Compression," International Journal of Impact Engineering, 37(2), Pages 141-149.

Kim, D-J., Naaman, A.E. and El-Tawil, S. (2010c), "Correlation between Tensile and Bending Behavior of FRC Composites with Scale Effect," Proceedings of FraMCoS-7, 7th International Conference on Fracture Mechanics of Concrete and Concrete Structures, May 23-28, 2010, Jeju Island, South Korea

Kim, D-J, Naaman, A. E. and El-Tawil, S. (2008a), "Comparative Flexural Behavior of Four Fiber Reinforced Cementitious Composites," Journal of Cement and Concrete Composites, Elsevier, Vol. 30, November 2008, pp.917-928.

Kim, D-J, El-Tawil, S. and Naaman, A. E. (2008b), "Rate-Dependent Tensile Behavior of High Performance Fiber Reinforced Cementitious Composites," Materials and Structures, RILEM, ISSN 1359-5997 (in print), 1871-6873 (online).

Kim, D-J, El-Tawil, S. and Naaman, A. E. (2008c), "Loading Rate Effect on Pullout Behavior of Deformed Fibers," ACI Materials Journal, 105(6), November-December 2008, pp.576-584

Kim, D-J, Naaman, A. E. and El-Tawil, S. (2008d), "High Tensile Strength Strain-Hardening FRC Composites with Less Than 2% Fiber Content," Proceedings of the Second International Symposium on Ultra High Performance Concrete, March 05 - 07, 2008, Kassel, Germany.

Kim, D-J, El-Tawil, S. and Naaman, A. E. (2007), "Correlation between Single Fiber Pullout and Tensile Response of FRC Composites with High Strength Steel Fibers," Proceedings of HPFRCC5, H. W. Reinhardt and A.E. Naaman Editors, July 10-13, Mainz, Germany.

Kok Seng Chia, Min-Hong Zhang, “Water permeability and chloride penetrability of high-strength lightweight aggregate concrete”, Cement and Concrete Research, 32 (2002) 639-645

Liu, Zhichao. FROST DETERIORATION IN CONCRETE DUE TO DEICING SALT EXPOSURE: MECHANISM, MITIGATION AND CONCEPTUAL SURFACE SCALING MODEL. Diss. U of Michigan, 2014. N.p.: n.p., n.d. Print.

Naaman, A. E., and H. W. Reinhardt. "Proposed Classification of HPFRC Composites Based on Their Tensile Response." Materials and Structures 39.5 (2007): 547-55. Web

Naaman, A.E., and Reinhardt, H.W., "Characterization of High Performance Fiber Reinfoced Cement Composites," in "High Performance Fiber Reinforced Cement Composites – HPFRCC 2,' A.E. Naaman and F.W. Reinhardt, Editors, RILEM Pb. 31, E. and FN Spon, England, 1996; pp. 1-24

Oertel, Tina, Frank Hutter, Ricarda Tänzer, Uta Helbig, and Gerhard Sextl. "Primary Particle Size and Agglomerate Size Effects of Amorphous Silica in Ultra-high Performance Concrete." Cement and Concrete Composites 37 (2013): 61-67. Web.

Piérard, J., Dooms, B., and Cauberg, N., “Evaluation of Durability Parameters of UHPC Using Accelerated Lab Tests,” Proceedings of Hipermat 2012 3rd Internationa Symposium on UHPC and Nanotechnology for High Performance Construction Materials, Ed., Schmidt, M., Fehling, E., Glotzbach, C., Fröhlich, S., and Piotrowski, S., Kassel University Press, Kassel, Germany, 2012, pp. 371–376.

Piotrowski, S. and Schmidt, M., “Life Cycle Cost Analysis of a UHPC-Bridge on Example of Two Bridge Refurbishment Designs,” Proceedings of Hipermat 2012 3rd International Symposium on UHPC and Nanotechnology for High Performance Construction Materials, Ed., Schmidt, M., Fehling, E., Glotzbach, C., Fröhlich, S., and Piotrowski, S., Kassel University Press, Kassel, Germany, 2012, pp. 957–964

Pyo, Sukhoon, Kay Wille, Sherif El-Tawil, and Antoine E. Naaman. "Strain Rate Dependent Properties of Ultra High Performance Fiber Reinforced Concrete (UHP-FRC) under Tension." Cement and Concrete Composites 56 (2015a): 15-24. Web.

Pyo, S., El-Tawil, S. (2015b), “Capturing the Strain Hardening and Softening Responses of Cementitious Composites Subjected to Impact Loading,” Journal of Construction and

Building Materials, Elsevier, 81(15), April 2015, pp. 276–283, doi:10.1016/j.conbuildmat.2015.02.028.

Pyo, S. and El-Tawil, S. (2013a), "Crack velocity-dependent dynamic tensile behavior of concrete", International Journal of Impact Engineering, V55, pp. 63-70, http://dx.doi.org/10.1016/ j.ijimpeng.2013.01.003.

Pyo, S. and El-Tawil, S. (2013b), "Dynamic Fracture Mechanics Based DIF Models for Concrete under Tensile Loading," 2013 Conference of the ASCE Engineering Mechanics Institute, August 4 – 7, 2013, Northwestern University, Evanston, IL

Pyo, S., El-Tawil, S. and Naaman, A.E. (2013c), "Parametric Study of a New Impact Testing System for Ultrahigh Performance Concrete in Tension," 2013 Conference of the ASCE Engineering Mechanics Institute, August 4 – 7, 2013, Northwestern University, Evanston, IL

Rigaud, Stephane, Phillippe Fonollosa, and Gilles Chanvillard. Concrete Composition. Lafarge, assignee. Patent US8303708 B2. 6 Nov. 2012. Print.

RILEM TC 176-IDC, M.J. Setzer, P. Heine, S. Kasparek, S. Palecki, R. Auberg, V. Feldrappe, E. Siebel, Test methods of frost resistance of concrete: CIF-Test: Capillary suction, internal damage and freeze thaw test)-Reference method and alternative methods A and B, Mater. Struct. 37 (274) (2004) 743-753.

Rong, Z.d., W. Sun, H.j. Xiao, and W. Wang. "Effect of Silica Fume and Fly Ash on Hydration and Microstructure Evolution of Cement Based Composites at Low Water–binder Ratios." Construction and Building Materials 51 (2014): 446-50. Web.

Rong, Zhidan, Wei Sun, Haijun Xiao, and Guang Jiang. "Effects of Nano-SiO2 Particles on the Mechanical and Microstructural Properties of Ultra-high Performance Cementitious Composites." Cement and Concrete Composites 56 (2015): 25-31. Web.

Saleem, Muhammad Azhar, Amir Mirmiran, Jun Xia, and Kevin Mackie. "Development Length of High-Strength Steel Rebar in Ultrahigh Performance Concrete." J. Mater. Civ. Eng. Journal of Materials in Civil Engineering 25.8 (2013): 991-98. Web.

Slater, W.a., F.e. Richart, and G.g. Scofield. "Tests of Bond Resistance between Concrete and Steel." Technologic Papers of the Bureau of Standards (1920): n. pag. Web

Steinberg, Eric. "Structural Reliability of Prestressed UHPC Flexure Models for Bridge Girders." Journal of Bridge Engineering 15 (2010): 65-72. Web.

Sutter, Lawrence L. Evaluation of Methods for Characterizing Air Void Systems in Wisconsin Paving Concrete. Madison, WI: Wisconsin Highway Research Program, 2007. Print

Swenty, M. and Graybeal, B., "Influence of Differential Deflection on Staged Construction Deck-Level Connections," FHWA, U.S. Department of Transportation, Report No. FHWAHRT-12-057, National Technical Information Service Accession No. PB2012-111528, 2012.

Tanesi, Jussara, and Richard Meininger. "Freeze-Thaw Resistance of Concrete with marginal Air Content." Transportation Research Record 2020.-1 (2007): 61-66. Web.

Wille, K., Kim, D., and Naaman, A.E., "Strain-Hardening UHP-FRC With Low Fiber Contents," Materials and Structures, Vol. 44, No. 3, 2011, pp. 583–598

Wille, K., Naaman, A.E., and El-Tawil, S., "Optimizing Ultra-High-Performance Fiber Reinforced Concrete," Concrete International, Vol. 33, No. 9, September 2011, pp. 35–41

Wille, K., Naaman, A.E., and Parra-Montesinos, G.J., "Ultra-High Performance Concrete With Compressive Strength Exceeding 150 MPa (22 ksi): A Simpler Way," ACI Materials Journal, Vol. 108, No. 1, January–February 2011, pp. 46–54.

Wille, Kay, and Antoinne Naaman. "Pullout Behavior of High-Strength Steel Fibers Embedded in Ultra-High-Performance Concrete." ACI Materials Journal MJ 109.4 (2012): n. pag. Web.

Wille, Kay, and Christopher Boisvert-Cotulio. "Material Efficiency in the Design of Ultra-high Performance Concrete." Construction and Building Materials 86 (2015): 33-43. Web.

Wille, Kay, and Gustavo Parra-Montesinos. "Effect of Beam Size, Casting Method, and Support Conditions on Flexural Behavior of Ultra-High-Performance Fiber-Reinforced Concrete." ACI Materials Journal MJ109.3 (2012): n. pag. Web.

Wille, Kay, Antoine E. Naaman, Sherif El-Tawil, and Gustavo J. Parra-Montesinos. "Ultra-high Performance Concrete and Fiber Reinforced Concrete: Achieving Strength and Ductility without Heat Curing." Mater Struct Materials and Structures 45.3 (2011): 309-24. Web.

Wille, Kay, Dong Joo Kim, and Antoine E. Naaman. "Strain-hardening UHP-FRC with Low Fiber Contents." Materials and Structures 44.3 (2011): 583-98. Web.

Wille, K., Xu, M., El-Tawil, S. and Naaman, A.E. (2015), "Dynamic Impact Factors of Strain Hardening UHP-FRC under Direct Tensile Loading at Low Strain Rates," Accepted for

publication in the RILEM Materials and Structures Journal. DOI: 10.1617/s11527-015-0581-y.

Wille, K., El-Tawil, S. and Naaman, A.E. (2014), "Properties of Strain Hardening Ultra High Performance Fiber Reinforced Concrete (UHP-FRC) under Direct Tensile Loading," Journal of Cement and Concrete Composites, Elsevier, 48, pp. 53-66, doi:10.1016/j.cemconcomp.2013.12.015

Wille, K., Naaman, A. E. and El-Tawil, S. (2011), "Ultra High Performance Fiber Reinforced Concrete (UHP-FRC) Record Performance under Tensile Loading," Concrete International, American Concrete Institute, Sept. 2011, pp. 35-41.

Wille, K., El-Tawil, S. and Naaman, A. E. (2011), "Strain Rate Dependent Tensile Behavior of Ultra-High Performance Fiber Reinforced Concrete," Proceedings of HPFRCC6, H. W. Reinhardt and G. Parra Editors, Ann Arbor, MI.

Wipf, T., Sritharan, Sri,., "Iowa's UHPC Implementation" Iowa Research, Bureau of Research and Technology, April, 2011

Yazıcı, Halit. "The Effect of Silica Fume and High-volume Class C Fly Ash on Mechanical Properties, Chloride Penetration and Freeze–thaw Resistance of Self-compacting Concrete." Construction and Building Materials 22.4 (2008): 456-62. Web.

Yu, R., P. Spiesz, and H.j.h. Brouwers. "Development of an Eco-friendly Ultra-High Performance Concrete (UHPC) with Efficient Cement and Mineral Admixtures Uses." Cement and Concrete Composites 55 (2015): 383-94. Web.

Yu, R., P. Spiesz, and H.j.h. Brouwers. "Development of Ultra-High Performance Fibre Reinforced Concrete (UHPFRC): Towards an Efficient Utilization of Binders and Fibres." Construction and Building Materials 79 (2015): 273-82. Web.

Yu, R., P. Spiesz, and H.j.h. Brouwers. "Effect of Nano-silica on the Hydration and Microstructure Development of Ultra-High Performance Concrete (UHPC) with a Low Binder Amount." Construction and Building Materials 65 (2014): 140-50. Web.

Intentionally left blank